ADVANCED FUNCTIONAL MATERIALS
www.afm-journal.de

Plasmon-Induced Pyro-Phototronic Effect Enhancement in Self-Powered UV–Vis Detection with a ZnO/CuO p–n Junction Device

*Qi Li, Jianping Meng, Jing Huang, and Zhou Li**

It is important to detect light of low power density sensitively and fast for the application of optical communication, environmental monitoring, astronomy, and national securities. However, ZnO-based photodetectors exhibit long decay time owing to the persistent photoconductivity (PPC) and are hard to detect light with low power density efficiently. Here, a practical strategy is utilized to improve the performance of ZnO-based photodetectors by coupling the pyroelectric effect of ZnO with localized surface plasmon resonance (LSPR) of Au nanoparticles subtly. Hence, a self-powered photodetector is demonstrated, which is integrated with ZnO/CuO core–shell nanorods and Au nanoparticles to detect UV to vis light. This self-powered photodetector achieves fast and sensitive detection of UV when power density is 68 nW cm^{-2}. The performance is significantly improved than the photodetectors without Au nanoparticles. The optimal responsivity and detectivity under the same power density of UV at 325 nm are 1.4×10^{-4} A W^{-1} and 3.3×10^{11} Jones. Response/recovery time is remarkably shortened to ≈10 ms. The results indicate that the material configurations and design concept make the device applicable for self-powered, high-performance photodetectors, and provide further promoted understanding of LSPR enhanced performance of photodetectors.

1. Introduction

The sensing of ultraviolet, visible, and infrared radiation is of scientific and technological importance for a wide range of applications that enable optical communications, ozone sensing, environmental monitoring, video imaging, astronomical exploration, etc.[1–3] For specific national securities, sensors designed for the ultraviolet spectral region may offer many advantages over longer wavelength systems aiming to monitor, identify, and track rockets or missiles.[4]

Several kinds of metal-oxide semiconductors have been applied in UV photodetectors to realize widespread application and various powerful strategies are used to enhance the performance of photodetectors.[5] ZnO with suitable bandgap of 3.37 eV has offered tantalizing possibilities for various unique functions and/or high-performance UV sensing devices.[6,7] 1D nanowires rendere intriguing physical and chemical properties, such as resonant light absorption, large surface to volume ratio, excellent mechanical flexibility, and so on.[8,9] The state-of-the-art photodetectors based on ZnO nanowires have been demonstrated remarkable increasement of performance such as detectivity, responsivity, and response/recovery time.[8,10–13]

However, inherent oxygen vacancies within the bandgap of ZnO leads to persistent photoconductivity (PPC),[14,15] which will prolong the recovery time noticeably. It is critical to solve this problem to allow rapid recovery. Constructing a p–n junction photodetector is an alternative way to optimize the performance of ZnO-based photodetectors.[16] On the one hand, it not only enables the efficient combination of spectral response range of materials with each other realizing broadband spectral detection but also presents additional synergistic properties.[17] On the other hand, a photodetector without an external bias is beneficial to device integration, avoiding extra cost and energy consumption.[18–20] Thus, self-powered devices facilitated by the photovoltaic effect of p–n junction are essential and significant to solve the issue.[21,22] Light-induced pyroelectric effect is a promising solution to optimize ZnO-based photodetectors.[10,12,23,24] Light-induced pyroelectric effect can modulate the carrier transmission and distribution in the semiconductor materials,[25] which will largely promote the performance of a photodetector with p–n

Q. Li, J. Meng, J. Huang, Z. Li
CAS Center for Excellence in Nanoscience
Beijing Key Laboratory of Micro-Nano Energy and Sensor
Beijing Institute of Nanoenergy and Nanosystems
Chinese Academy of Sciences
Beijing 101400, China
E-mail: zli@binn.cas.cn

Q. Li, J. Huang
College of Chemistry and Chemical Engineering
Guangxi University
Nanning 530004, China

Q. Li, J. Huang, Z. Li
Center on Nanoenergy Research
School of Physical Science and Technology
Guangxi University
Nanning 530004, China

J. Meng, Z. Li
School of Nanoscience and Technology
University of Chinese Academy of Sciences
Beijing 100049, China

The ORCID identification number(s) for the author(s) of this article can be found under https://doi.org/10.1002/adfm.202108903.

DOI: 10.1002/adfm.202108903

heterojunction. Meanwhile, self-powered pyroelectric photodetection can be realized to obtain better performance.[26] Especially, pyroelectric potential produced by pyro-polarization charges can eliminate adverse effects of PPC rapidly and intentionally like a positive gate voltage.[15] Pyroelectric current is dependent on the power density of incident light at a certain temperature. Detection of light of low power density is prohibitive due to the weak pyroelectric current. We need to devote efforts to improve that performance. Therefore, it is necessary for some new strategies and working mechanisms to improve detection performance of ZnO-based photodetectors across the board. As is known that pyroelectric current is proportional to rate of temperature change.[27] Exactly, localized surface plasmon resonance (LSPR) produces transient thermal power to raise temperature fast.[28–30]

In this paper, a self-powered photodetector based on p–n junction of n-ZnO and p-CuO was designed by coupling with the LSPR-enhanced pyroelectric effect and photovoltaic effect. It realized highly sensitive detection for UV light with low power density of 68 nW cm^{-2}. Additionally, the detection waveband of the photodetector was widened from UV to vis radiation.

2. Results and Discussions

The schematic of the strategy to prepare the photodetector device composed of vertically aligned ZnO/CuO core/shell nanorods and Au nanoparticles (NPs) was illustrated by a four-step method (**Figure 1**a) with the fabricating process detailed in the Experimental Section. A ZnO seed layer was deposited on the substrate and then a hydrothermal method was utilized to grow ZnO nanorods. ZnO nanorods were ≈9.3 µm long (Figure S1a, Supporting Information). ZnO nanorods were covered by CuO through reaction in a solution and scanning electron microscope (SEM) image of the products remained uniform with nanorod morphology but the nanowires changing from smooth surfaces to rough surfaces (Figure S1b, Supporting Information). It indicated a core/shell structure of each CuO-coated ZnO nanorod partly. Last, Au NPs were decorated on each CuO-coated ZnO nanorod and then silver paste and F-doped tin oxide (FTO) substrate were used as the top electrode and bottom electrode, respectively. The energy band diagram of the ZnO/CuO/Au device relative to the vacuum energy level respectively indicated that the p–n heterostructure had a staggered energy band configuration (Figure 1b).

X-ray diffractometer (XRD) and Raman spectra of the nanorods at room temperature (Figure 1c,d) pointed out that there were two components in the nanorods containing ZnO and CuO. A slight increase in absorption was noticed for ZnO/CuO core/shell nanorods compared with original ZnO nanorods (Figure 1d). After decorating Au NPs on the surface of ZnO/CuO core/shell nanorods, absorption in the region of

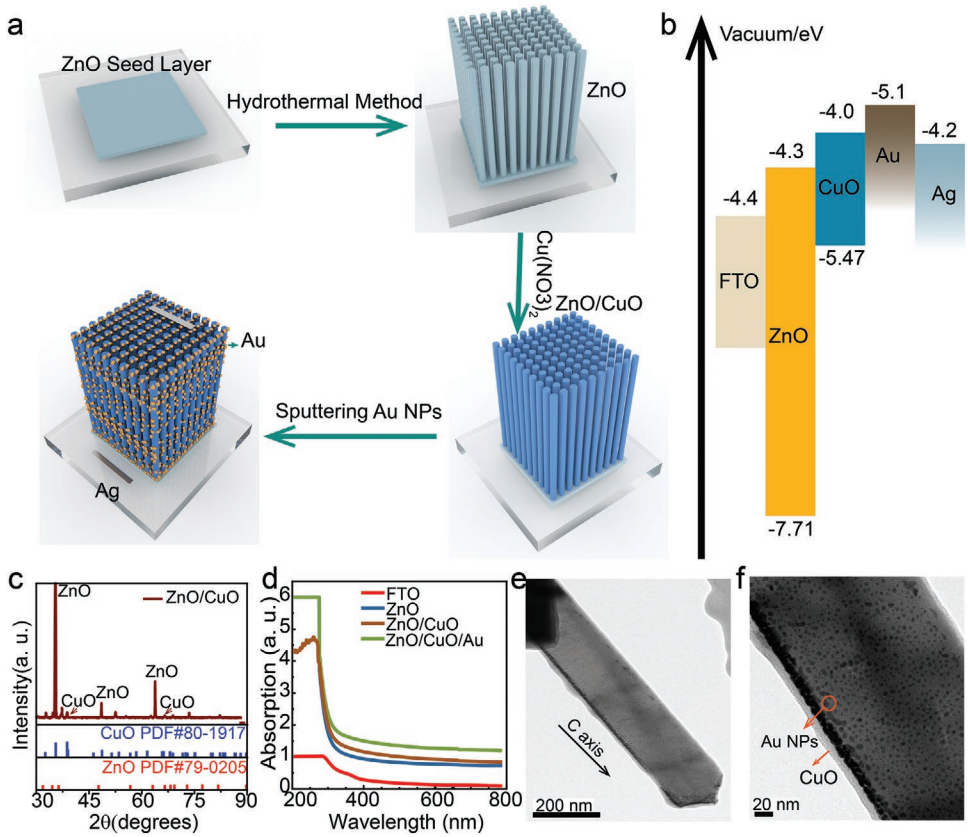

Figure 1. Device structure and basic characterization of self-powered p-CuO/n-ZnO/Au NPs photodetector. a) Schematic of preparation process for vertically aligned ZnO/CuO/Au NPs core/shell nanorods photodetector device. b) Energy band diagram of a self-powered ZnO/CuO/Au photodetector. c) XRD patterns of ZnO/CuO. d) UV–vis–NIR absorption spectra of components of the photodetector. e) TEM image and f) the corresponding enlarged TEM image of single ZnO/CuO/Au NPs core/shell nanorod (Au loadings of 230 nmol).

200–800 nm enhanced further. Transmittance and reflectance spectra indicated that ZnO/CuO/Au had the lowest transmittance and reflectance in the region of 250–800 nm compared with ZnO/CuO and ZnO (Figure S2, Supporting Information). Light harvesting efficiency (LHE) was defined to achieve quantitative description of the light absorption capability of the materials. It can be calculated as LHE = 1 − transmittance% − reflectance%.[31] LHE of ZnO/CuO was much stronger than ZnO and reached ≈70% around 400–700 nm, owing to enhancement of light absorption by coating ZnO nanorods with CuO. After decorating Au NPs, ZnO/CuO/Au displayed prominently raised LHE compared with ZnO and ZnO/CuO. The maximum LHE of ZnO/CuO/Au was 96.6% around 300 nm. Au NPs can enhance LHE of the materials dramatically. The trap structure constructed with ZnO/CuO nanorods was of benefit to absorption of light. As the radius of an Au NP was less than ≈30 nm, light absorption dominated over light scattering.[32] When Au NPs were close to the interface between two dielectrics, light was preferentially scattered into dielectric with the larger permittivity and then light was trapped into the semiconductor.[33] Meanwhile, light will be trapped in these materials for angle beyond the critical angle for reflection.[33] Moreover, it should be noted that LSPR produced by Au NPs can enhance absorption of light and the efficiency of photothermal conversion.[34] Hence, Au NPs can enhance LHE of the materials efficiently. Photoluminescence spectra for ZnO, ZnO/CuO, and ZnO/CuO/Au (Figure S3c, Supporting Information) exhibited emission at 456 nm. The peak intensity of ZnO/CuO was pretty small than ZnO and approached that of ZnO/CuO/Au. Broad visible luminescence (centra at 561 nm) from 480 to 700 nm. The two peaks indicated various deep level defects such as oxygen interstitials and oxygen vacancies and surface states in ZnO.[35] After coating ZnO nanorods with CuO shell and Au NPs, the peaks decreased dramatically and rarely shifted, which demonstrated that CuO and Au NPs passivated the surface defects of ZnO nanorods. Importantly, the hot holes from LSPR were able to recombine with the electrons present at the V_o^x, V_o^+ states. ZnO defect levels were usually beyond that of the hot hole levels. Thus, these defect level electrons recombined with hot holes through this energetically favorable path, causing suppression of defect-related visible emissions.[36]

Obviously, Figure 1e,f illustrated that a single ZnO/CuO/Au nanorod was a composite where a uniform CuO layer (thickness of 2 nm) was coated on the ZnO nanorod (diameter of 100 nm). Au NPs with a diameter of ≈3 nm were distributed on the surface of ZnO/CuO core/shell nanorods (Figure 1f). Interplanar distance of 0.52 nm measured from high-resolution transmission electron microscope (TEM) image (Figure S4a, Supporting Information) was corresponding to double lattice fringes of ZnO (002). Elements of Zn, O, Cu, and Au were confirmed by energy dispersive spectroscopy (EDS) (Figure S4b,c, Supporting Information). We can conclude that ZnO/CuO/Au NP nanorods were obtained by conducting an easy method.

Typical nonlinear *I–V* curves of the photodetectors based on ZnO–CuO p–n junction before and after loading Au NPs suggested excellent UV response at the positive voltages and rectification characteristics (Figure S5a–g, Supporting Information). Liner *I–V* curve of the Ag/CuO device demonstrated ohmic contact formed between Ag and CuO (Figure S5h, Supporting Information). *I–t* curves of photodetectors were captured at zero bias under illumination of 325 and 532 nm with power density ranging from 68 nW cm^{-2} to 6.8 μW cm^{-2} (**Figure 2**a–c). ZnO/CuO devices exhibited weak photoresponse even power density of 325 nm illumination was 3.4 μW cm^{-2} (Figure 2a). The output current of photodetector increased monotonously as power density of 325 or 532 nm laser rose, because electron–hole pairs excited by photons increased. The sharp peak of output current at rise and fall step was the feature of light-induced pyroelectric effect.[17]

Comparing to ZnO/CuO devices, it was found that ZnO/CuO/Au NP devices (all the Au loading ranging from 57 to 344 nmol) exhibited transient pyroelectric current under illumination of 325 nm laser with power density of 6.8 μW cm^{-2} (**Figure 3**a). The similar experiment for 532 nm radiation was also conducted (Figure 3b). The devices with Au loading of 287 nmol were able to detect 532 nm light with a good signal to noise ratio. Responsivity (*R*) and detectivity (*D**) were used as important parameters to describe the sensitivity of a photodetector.[11] Detectivity went up initially, and then decreased. The maximal transient responsivity and detectivity of the photodetector with Au loading of 287 nmol were 5.07×10^{-5} A W^{-1} and 4.53×10^9 Jones under illumination of 325 nm laser, respectively (Figure 3c). The response/recovery time was decreased from 329.6/403.7 ms to 6.3/6.9 ms after devices being decorated Au of 230 nmol (Figure 3d), indicating response/recovery time shortened noticeably. The similar phenomenon was also found to 532 nm laser (Figure 3e).

Current enhancement factor β was defined to better demonstrate the performance of devices as $\beta = I_p/I_d$, where $I_p = I_t - I_d$, where I_t and I_d are the transient pyroelectric current and dark current of the photodetector, respectively. After loading Au of 287 nmol, the obtained photodetectors demonstrated a peak specific current enhancement factor β, responsivity *R*, and detectivity *D** of 55.9, 9.4×10^{-8} A W^{-1}, and 8.4×10^7 Jones (Figure S10, Supporting Information). All the parameters to represent strength of device detection capabilities were improved significantly for 325 nm laser. Current enhancement factor β, responsivity, and detectivity at 287 nmol was 169 times, twice, and 18 times that of ZnO/CuO devices, respectively. Moreover, the response/recovery time was decreased from 287.8/1465 ms to 11.6/12.7 ms after devices being sputtered Au of 287 nmol (Figure 3e). All these results proved that the plasmonic Au played a key role in improving the performance of the self-powered CuO/ZnO/Au photodetector. Critical roles of Au NPs were also confirmed by finite difference time domain simulation (Figure S11, Supporting Information).

The device with Au loading of 230 nmol can achieve high-sensitive detection to 325 nm laser with low power density of 68 nW cm^{-2} (**Figure 4**a). However, ZnO/CuO devices were not able to detect even the power density reached to 360 nW cm^{-2} (Figure 4b). β, *R*, and *D** displayed an increasement first and then a decrease as a function of Au loading (Figure 4c,d). The peak β and *D** were obtained as 19.6 and 3.3×10^{11} Jones, respectively, for devices with Au loading of 230 nmol. Peak responsivity was obtained as 1.74×10^{-4} A W^{-1} at 172 nmol. Current enhancement factor β of all the ZnO/CuO/Au photodetectors were larger than that of ZnO/CuO devices. In case of light illumination of 6.8 μW cm^{-2}, the maximal enhancement

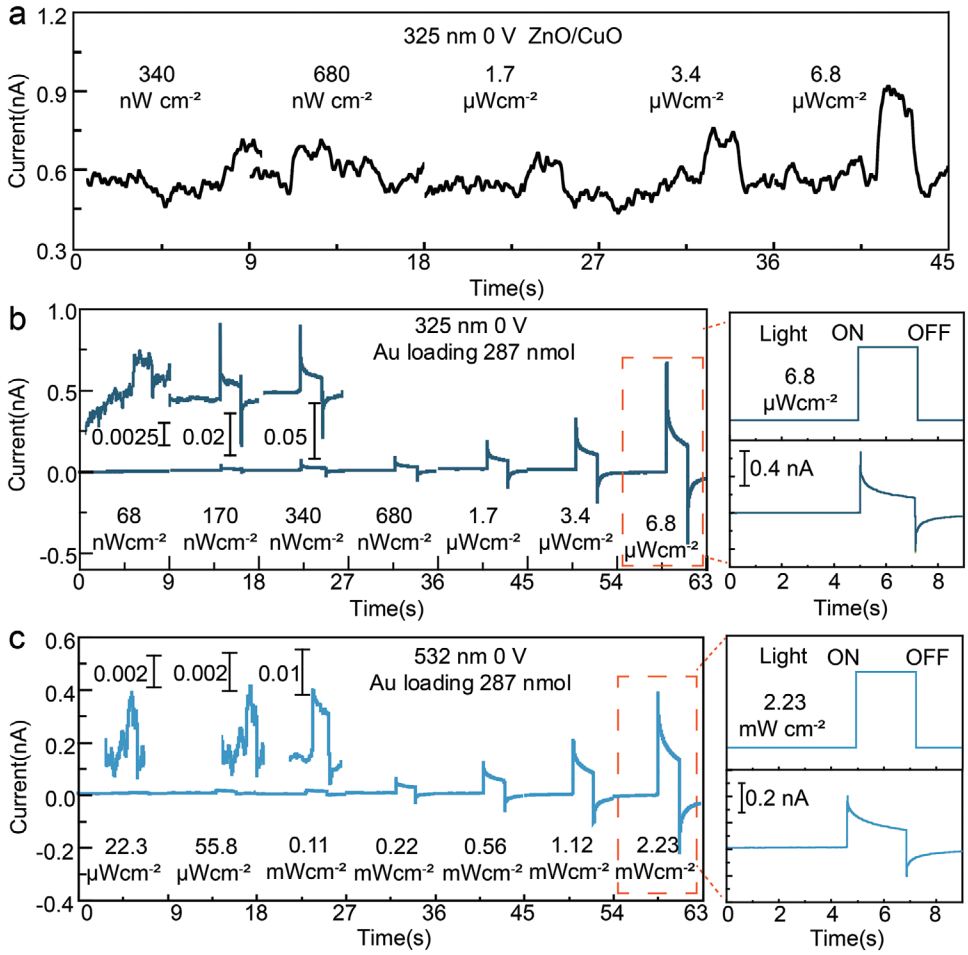

Figure 2. Photoresponse of CuO/ZnO/Au NP photodetectors. a) *I–t* characteristics of CuO/ZnO photodetectors under 325 nm illumination with different power densities from 340 nW cm^{-2} to 6.8 μW cm^{-2} without external bias. b) *I–t* characteristics of CuO/ZnO/Au NP photodetectors loading Au of 287 nmol under 325 nm illumination with different power densities from 68 nW cm^{-2} to 6.8 μW cm^{-2} without external bias and corresponding pulsed-light-induced transient pyroelectric current. c) *I–t* characteristics of CuO/ZnO/Au NP photodetectors loading Au of 287 nmol under 532 nm illumination with different power densities from 22.3 μW cm^{-2} to 2.23 mW cm^{-2} without external bias and corresponding pulsed-light-induced transient pyroelectric current. Active area of the devices was 1.3 × 1.3 cm^2.

factor β can be obtained as 217.2 for ZnO/CuO/Au photodetectors with Au loading of 230 nmol under illumination of 325 nm light with power density of 6.8 μW cm^{-2} (Figure 4c), which was 412.3 times that of ZnO/CuO devices (0.53). It indicated that the LSPR can greatly improve even optimize the performance of the ZnO/CuO/Au photodetectors for 325 nm photon sensing. The device with Au loading of 230 nmol was also used in the measurement of spectral photoresponse to obtain the detection limit of the illumination signal, where the responsivity varied in the spectral range from 325 to 1030 nm (Figure S12, Supporting Information). The device displayed strong photoresponse in the spectral range from 325 to 400 nm and showed weak response to light from 450 to 550 nm. Whereas a peak of responsivity still can be observed at 532 nm in the enlarged image of inset in Figure S12 in the Supporting Information. These results revealed that it was effective to optimize performance by controlling the loading of Au NPs and further modulating charges and energy transfer in plasmonic Au–CuO semiconductors interface. Furthermore, some Au NPs might contact with each other as the Au loading increased properly so that collective excitation of metal NPs enhanced the utilization of plasmonic energy.[28] However, Au NPs can scatter light more efficiently but absorb light less due to a gain of radius as Au loading enhanced further when the radius of a particle exceeded 30 nm.[32] Consequently, the excellent devices were obtained as Au loading increased for the longish sputtering time was applied, and the performance degraded as the time increased further.

It was a four-stage photoresponse behavior for a ZnO/CuO/Au photodetector at zero bias (**Figure 5**a). Temperature increased once the light illuminated on the photodetector. Meanwhile, LSPR induced by Au NPs on the surface of CuO generated transient thermal power facilitating change of temperature at the moment of light illumination (in picosecond range[27,37]), which gave rise to positive pyroelectric charges at n side of p–n heterojunction and promoted the increase of pyroelectric current (Figure 5b). The positive polarization charges generated in ZnO nanorods within p–n heterojunction bent

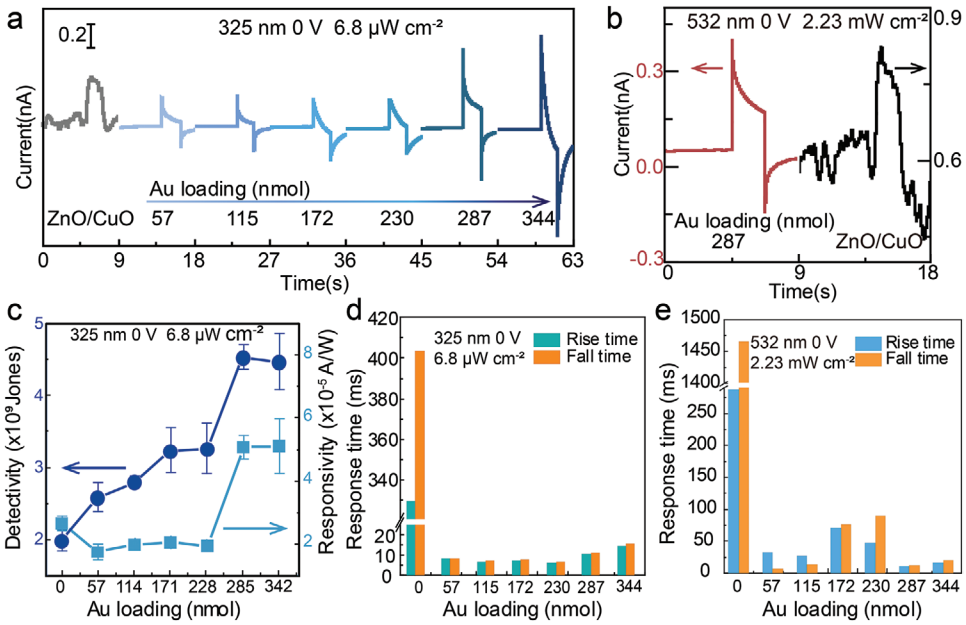

Figure 3. LSPR enhanced performances on UV detecting of self-powered ZnO/CuO/Au NP photodetectors. a) *I–t* characteristics of CuO/ZnO photodetectors and CuO/ZnO/Au NP photodetectors with variously loading Au from 57 to 344 nmol under 325 nm illumination (6.8 μW cm^{-2}) without external bias. b) *I–t* characteristics of CuO/ZnO photodetectors and CuO/ZnO/Au NP photodetectors loading Au of 287 nmol under 532 nm illumination (2.23 mW cm^{-2}) without external bias. c) Responsivity and detectivity of CuO/ZnO photodetectors and CuO/ZnO/Au NP photodetectors with various Au loading from 57 to 344 nmol under 325 nm illumination (6.8 μW cm^{-2}) without external bias. d,e) Response time of the photodetectors under 325 nm illumination (6.8 μW cm^{-2}) and under 532 nm illumination (2.23 mW cm^{-2}), respectively. Active area of the devices was 1.3 × 1.3 cm^2.

downward the energy band diagram resulting in the increase of the barrier height of the ZnO/CuO p–n junction,[23] which in turn effectively enhanced separation of the photogenerated charge carriers. Moreover, plasmonic hot electrons would enhance or generate the internal photoemission in photodetectors, and they were involved into photocurrent resulting in enhancement of the photoresponse intensity.[37] All the three factors made the total transient current larger after the devices loading Au NPs for coupling the photoelectric effect, pyroelectric effect, and LSPR. The output current would dramatically decrease and reach a plateau as the transient pyroelectric polarization degraded and photocurrent only originated from photovoltaic effect for temperature of ZnO nanorods changing to a stable state quickly. When the illumination was turned off, negative pyroelectric polarization charges were generated in the p–n junction of the photodetector and the energy band diagram bent upward at the ZnO side.[23] At the same time, a strong reversed current was observed owing to the reversed pyrocharges induced as instantaneous temperature decreased. Finally, the temperature of devices fell back to room temperature and remained steady without the laser irradiation, thus the output current returned to dark current with degradation of the pyroelectric current.

We have systematically investigated and thoroughly analyzed the local surface plasmon resonance of Au NPs interacting with pyroelectric effect and photovoltaic effect in a self-powered photodetector. The detection performance of devices was found to be much better after loading Au NPs. It was noticed that the response speed for the regular device was rather slow. The rise time decreased from 329.6 ms of ZnO/CuO devices to 6.3 ms of ZnO/CuO/Au devices, shortening to 52 times for plasmonic properties of Au NPs. Moreover, other performance parameters like detectivity and responsivity were also improved in the photodetectors with Au NPs. Such a great boost in response speed or other parameters were probably attributed to a faster increasement of temperature for LSPR induced by Au NPs. Uniquely, ZnO exhibited increased pyroelectric coefficients when heated below 430 K.[38] Thus, response time shortened and transient pyroelectric current increased significantly. More importantly, detection of ultraviolet with ultralow power density was achieved in the self-powered photodetector. It was a very crucial property for photodetectors to be applied in some fields such as optical communication and imaging. Because we designed the photodetector not only to exploit hot carrier generation but to use plasmonic heat effect, which made it fully take advantage of plasmonic energy for the two mechanisms better coupling with photovoltaic effect and pyroelectric effect. Plasmonic heat effect was one of the plasmonic energy transfer mechanisms which was seldom reported in photodetection, especially in UV detection. However, hot carrier generation and other energy transfer mechanisms were caught much attention and used to improve photodetector performance.[37,39–41] All these results demonstrated a new strategy to develop the energy utilization efficiency of plasmons and further facilitating the improvement of photodetector performance.

3. Conclusion

In summary, a self-powered photodetector integrated with ZnO/CuO core–shell nanorods and Au NPs was demonstrated to detect UV light to visible light although the power density

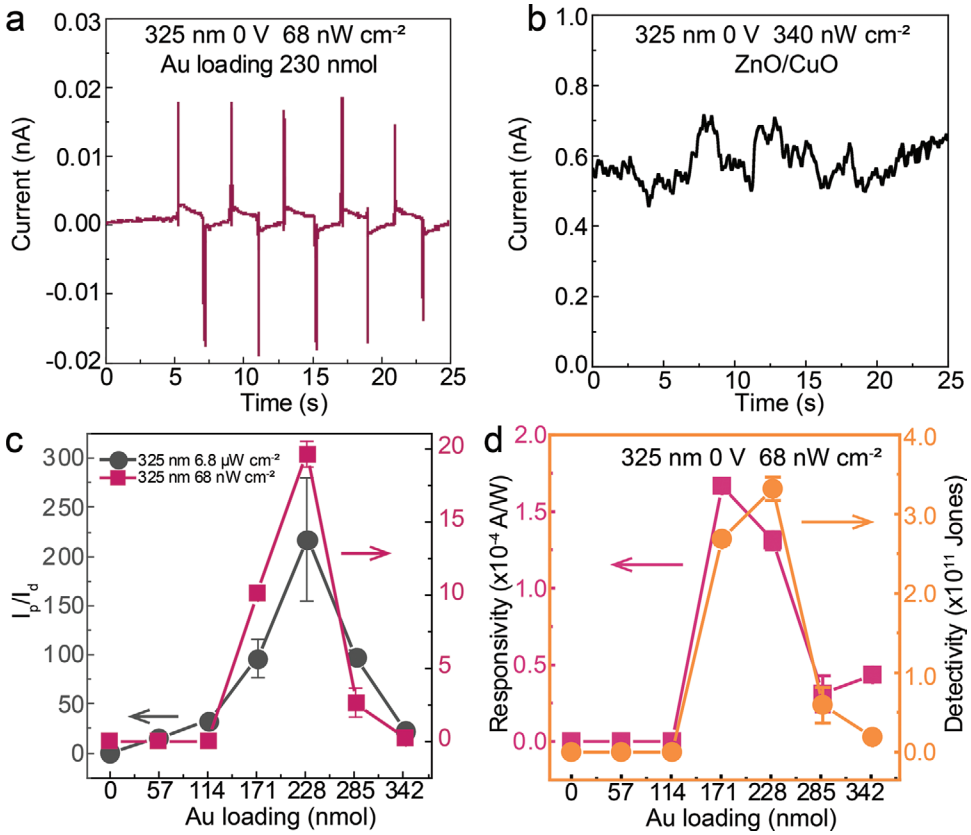

Figure 4. LSPR enhanced performances on ultralow power density light detecting of self-powered ZnO/CuO/Au NP photodetectors. a) *I–t* characteristics and CuO/ZnO/Au NP photodetectors with various Au loading from 57 to 344 nmol under 325 nm illumination (68 nW cm^{-2}) without external bias. b) *I–t* characteristics of CuO/ZnO photodetectors under 325 nm illumination (340 nW cm^{-2}) without external bias. c) Corresponding current enhancement index under 6.8 μW cm^{-2} and 68 nW cm^{-2} illumination of 325 nm, respectively. d) Responsivity and detectivity of the photodetectors with various Au loading from 57 to 344 nmol under 325 nm illumination (68 nW cm^{-2}) without external bias. Active area of the devices was 1.3 × 1.3 cm^2.

of UV light was as low as 68 nW cm^{-2}—a value was rarely observed in other ZnO-based photodetectors. The unique configuration of the photodetector combined the pyroelectric and photovoltaic effects with localized surface plasmon resonance, which suggested the excellent performance of the photodetector. The responsivity and detectivity for 325 nm light of 68 nW cm^{-2} were 1.4×10^{-4} A W^{-1} and 3.3×10^{11} Jones for devices with Au loading of 230 nmol, while the devices without Au NPs cannot detect even more large light power density at 360 nW cm^{-2}. An elaborate design of the photodetector made it a perfect absorber with light trapping of nanorods and highly efficient utilization of plasmonic energy. We believe that prominent comprehensive performance of the photodetector has potential application in national securities, optical communication, and imaging. Meanwhile, the rationale discovered in this work probably is a cornerstone to design high-performance photodetectors using other nanomaterial systems as well.

4. Experimental Section

Device Fabrication: The prepatterned FTO glass substrates were cleaned by deionized water, acetone, and alcohol before the ZnO layer deposition. Then, the ZnO layer was deposited by magnetron sputtering machine (Denton Discovery 635) at room temperature. A simple hydrothermal method was used to synthesize ZnO nanorods. And then, ZnO nanorods were immersed in a solution with the addition of 2 mL NaOH (0.1 M), 2 mL $Cu(NO_3)_2$ (0.1 M), 2 mL $NH_4{\cdot}H_2O$ (5 M), and 18 mL H_2O and heated at 80 °C for 40 min to obtain core–shell ZnO/CuO nanorods. Finally, Au NPs were sputtered on surface of CuO for various loading from 57 to 344 nmol with current 20 mA by 108 Auto Cressington sputter coater at room temperature.

Material Characterization: Detailed microscopic structures of ZnO NWs, ZnO/CuO core–shell nanorods, and ZnO/CuO/Au core–shell nanorods were characterized using scanning electron microscope (Hitachi SU8020), transmission electron microscope, and high-resolution transmission electron microscope (Tecnai G^2 F20) as well as corresponding energy dispersive spectrometer at room temperature. Crystal and elementary composition were analyzed by X ray diffractometer (PANalytical X'Pert) with Cu K_α radiation, Raman spectra equipped with an Ar laser working at wavelength of 532 nm (LabRAM HR Evolution, Horiba) at room temperature. Absorption, transmittance, and reflectance spectra were conducted by Shimadzu UV3600 at room temperature.

Optical and Electrical Measurements: LED (MLED4-4) with emission from 365 to 1030 nm and monochromatic 325 nm lasers (KIMMON IK330IR-G) and 532 nm lasers (Laser Quantum, ventus 532) were used as light source. A continuously variable filter was used to tune the light power density. The corresponding power density was measured by digital power meters (Thorlab PM100D and Newport 818 P-001-12). The *I–V* characteristics for the photodetectors were performed by Keithley 4200 semiconductor analyzer. *I–t* characteristics of devices were

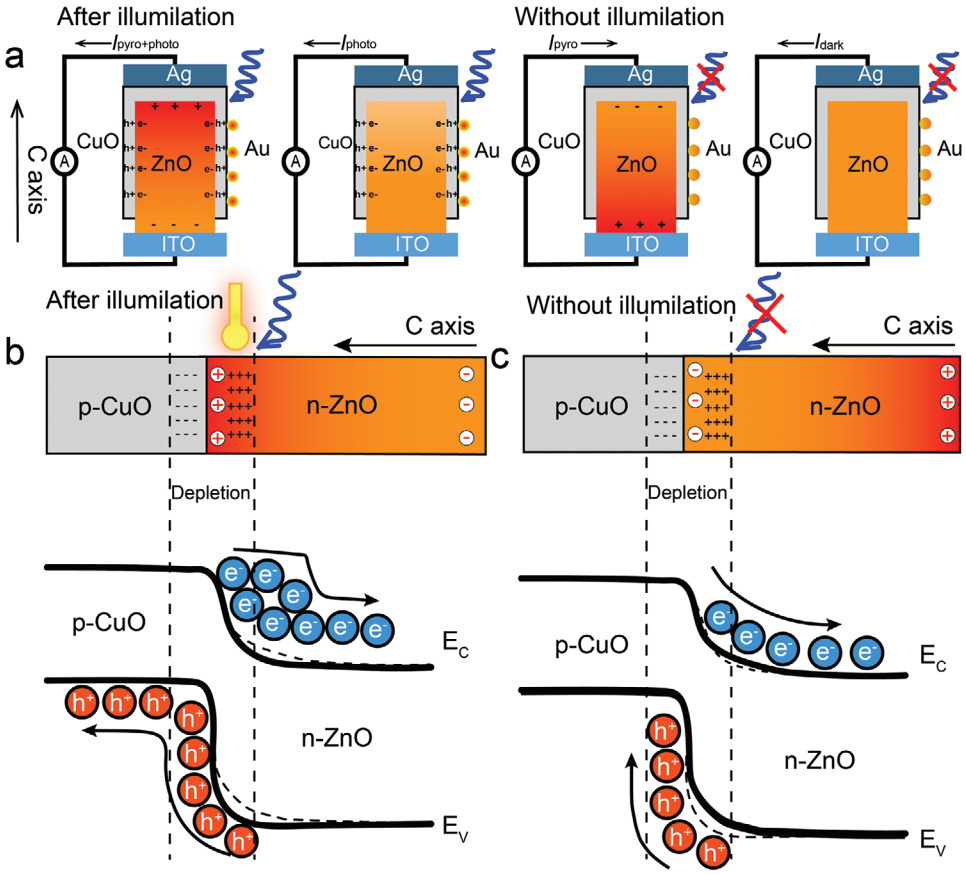

Figure 5. Working mechanism of self-powered photodetectors. a) Schematic illustration of the working mechanism of LSPR-combined pyroelectric and photoexcitation processes, corresponding to the four stages of photoresponse. b) Band diagrams of p-CuO/n-ZnO heterojunction at the moment of turning on light. c) Band diagrams of p-CuO/n-ZnO heterojunction at the moment of turning off light.

recorded by a LeCroy oscilloscope and a Keithley 6517B high resistance electrometer.

Supporting Information

Supporting Information is available from the Wiley Online Library or from the author.

Acknowledgements

Q.L. and J.M. contributed equally to this work. The authors are thankful for the support provided by the National Natural Science Foundation of China (52002027, T2125003, and 61875015), the Beijing Natural Science Foundation (2214083 and JQ20038), and the Youth Backbone Individual Project of Beijing Excellent Talents Training (Y9QNGG0501).

Conflict of Interest

The authors declare no conflict of interest.

Data Availability Statement

Research data are not shared.

Keywords

core–shell ZnO/CuO, low power density, plasmon-enhanced pyroelectric, self-powered photodetector

Received: September 3, 2021
Revised: October 15, 2021
Published online:

[1] F. Teng, K. Hu, W. Ouyang, X. Fang, *Adv. Mater.* **2018**, *30*, 1706262.
[2] H. Chen, H. Liu, Z. Zhang, K. Hu, X. Fang, *Adv. Mater.* **2016**, *28*, 403.
[3] K. Hu, F. Teng, L. Zheng, P. Yu, Z. Zhang, H. Chen, X. Fang, *Laser Photonics Rev.* **2017**, *11*, 1600257.
[4] C. E. Kolb, S. B. Ryali, J. C. Wormhoudt, in *Ultraviolet Technology II*, Vol. *932* (Ed: R. E. Huffman), SPIE, Washington, USA **1988**, p. 2.
[5] T. Zhai, X. Fang, M. Liao, X. Xu, H. Zeng, B. Yoshio, D. Golberg, *Sensors* **2009**, *9*, 6504.
[6] J. Meng, Z. Li, *Adv. Mater.* **2020**, *32*, 2000130.
[7] B. D. Boruah, *Nanoscale Adv.* **2019**, *1*, 2059.
[8] X. Liu, L. Gu, Q. Zhang, J. Wu, Y. Long, Z. Fan, *Nat. Commun.* **2014**, *5*, 4007.
[9] J. Meng, H. Li, L. Zhao, J. Lu, C. Pan, Y. Zhang, Z. Li, *Nano Lett.* **2020**, *20*, 4968.
[10] Z. Wang, R. Yu, X. Wang, W. Wu, Z. L. Wang, *Adv. Mater.* **2016**, *28*, 6880.

[11] Y. Zhang, M. Hu, Z. Wang, *Nano Energy* **2020**, *71*, 104630.
[12] Y. Wang, L. Zhu, Y. Feng, Z. Wang, Z. L. Wang, *Adv. Funct. Mater.* **2018**, *29*, 1807111.
[13] Y. Feng, Y. Zhang, Y. Wang, Z. Wang, *Nano Energy* **2018**, *54*, 429.
[14] Y. K. Su, S. M. Peng, L. W. Ji, C. Z. Wu, W. B. Cheng, C. H. Liu, *Langmuir* **2010**, *26*, 603.
[15] S. Jeon, S. Ahn, I. Song, C. J. Kim, U. Chung, E. Lee, I. Yoo, A. Nathan, S. Lee, K. Ghaffarzadeh, J. Robertson, K. Kim, *Nat. Mater.* **2012**, *11*, 301.
[16] W. Ouyang, F. Teng, J. He, X. Fang, *Adv. Funct. Mater.* **2019**, *29*, 1807672.
[17] D. You, C. Xu, W. Zhang, J. Zhao, F. Qin, Z. Shi, *Nano Energy* **2019**, *62*, 310.
[18] Y. Zhang, M. Peng, Y. Liu, T. Zhang, Q. Zhu, H. Lei, S. Liu, Y. Tao, L. Li, Z. Wen, X. Sun, *ACS Appl. Mater. Interfaces* **2020**, *12*, 19384.
[19] Z. Zhang, Y. Ning, X. Fang, *J. Mater. Chem. C* **2019**, *7*, 223.
[20] Y. Ning, Z. Zhang, F. Teng, X. Fang, *Small* **2018**, *14*, 1703754.
[21] J. Dong, Z. Wang, X. Wang, Z. L. Wang, *Nano Today* **2019**, *29*, 100798.
[22] B. D. Boruah, S. N. Majji, A. Misra, *Nanoscale* **2017**, *9*, 4536.
[23] W. Peng, X. Wang, R. Yu, Y. Dai, H. Zou, A. C. Wang, Y. He, Z. L. Wang, *Adv. Mater.* **2017**, *29*, 1606698.
[24] Z. Wang, R. Yu, C. Pan, Z. Li, J. Yang, F. Yi, Z. L. Wang, *Nat. Commun.* **2015**, *6*, 8401.
[25] W. Wu, Z. L. Wang, *Nat. Rev. Mater.* **2016**, *1*, 16031.
[26] B. B. Deka, M. S. Naidu, S. Nandi, A. Misra, *Nanoscale* **2018**, *10*, 3451.
[27] J. W. Stewart, J. H. Vella, W. Li, S. Fan, M. H. Mikkelsen, *Nat. Mater.* **2020**, *19*, 158.
[28] G. Yu, J. Qian, P. Zhang, B. Zhang, W. Zhang, W. Yan, G. Liu, *Nat. Commun.* **2019**, *10*, 4912.
[29] X. Chen, Y. Chen, M. Yan, M. Qiu, *ACS Nano* **2012**, *6*, 2550.
[30] A. O. Govorov, H. H. Richardson, *Nano Today* **2007**, *2*, 30.
[31] B. Deka Boruah, A. Misra, *ACS Appl. Mater. Interfaces* **2016**, *8*, 18182.
[32] M. Rycenga, C. M. Cobley, J. Zeng, W. Li, C. H. Moran, Q. Zhang, D. Qin, Y. Xia, *Chem. Rev.* **2011**, *111*, 3669.
[33] H. A. Atwater, A. Polman, *Nat. Mater.* **2010**, *9*, 205.
[34] J. Li, S. K. Cushing, F. Meng, T. R. Senty, A. D. Bristow, N. Wu, *Nat. Photonics* **2015**, *9*, 601.
[35] T. Dixit, I. A. Palani, V. Singh, *J. Phys. Chem. C* **2017**, *121*, 3540.
[36] Y. Lin, C. Tsai, Y. Lu, C. Liu, *J. Appl. Phys.* **2006**, *99*, 093501.
[37] H. Tang, C. Chen, Z. Huang, J. Bright, G. Meng, R. Liu, N. Wu, *J. Chem. Phys.* **2020**, *152*, 220901.
[38] G. Heiland, H. Ibach, *Solid State Commun.* **1966**, *4*, 353.
[39] W. Li, J. G. Valentine, *Nanophotonics* **2017**, *6*, 177.
[40] C. de Melo, M. Jullien, Y. Battie, A. E. Naciri, J. Ghanbaja, F. Montaigne, J. Pierson, F. Rigoni, N. Almqvist, A. Vomiero, S. Migot, F. Mücklich, D. Horwat, *ACS Appl. Mater. Interfaces* **2018**, *10*, 40958.
[41] M. Chen, L. Shao, S. V. Kershaw, H. Yu, J. Wang, A. L. Rogach, N. Zhao, *ACS Nano* **2014**, *8*, 8208.